# Short period, high field cryogenic undulator for extreme performance x-ray free electron lasers

F. H. O'Shea,[1,*] G. Marcus,[1] J. B. Rosenzweig,[1,†] M. Scheer,[2] J. Bahrdt,[2] R. Weingartner,[3] A. Gaupp,[2] and F. Grüner[3]

[1]*Department of Physics, University of California, Los Angeles, California 90095, USA*
[2]*Helmholtz-Zentrum Berlin für Materialien und Energie, 14109 Berlin, Germany*
[3]*Department of Physics, Ludwig-Maximilians-Universität, 85748 Garching, Germany*

(Received 9 March 2010; published 13 July 2010)

Short period, high field undulators can enable short wavelength free electron lasers (FELs) at low beam energy, with decreased gain length, thus allowing much more compact and less costly FEL systems. We describe an ongoing initiative to develop such an undulator based on an approach that utilizes novel cryogenic materials. While this effort was begun in the context of extending the photon energy regime of a laser-plasma accelerator based electron source, we consider here implications of its application to sub-fs scenarios in which more conventional injectors are employed. The use of such low-charge, ultrashort beams, which has recently been proposed as a method of obtaining single-spike performance in x-ray FELs, is seen in simulation to give unprecedented beam brightness. This brightness, when considered in tandem with short wavelength, high field undulators, enables extremely high performance FELs. Two examples discussed in this paper illustrate this point well. The first is the use of the SPARX injector at 2.1 GeV with 1 pC of charge to give 8 GW peak power in a single spike at 6.5 Å with a photon beam peak brightness greater than $10^{35}$ photons/(s mm$^2$ mrad$^2$ 0.1% BW), which will also reach LCLS wavelengths on the 5th harmonic. The second is the exploitation of the LCLS injector with 0.25 pC, 150 as pulses to lase at 1.5 Å using only 4.5 GeV energy; beyond this possibility, we present start-to-end simulations of lasing at unprecedented short wavelength, 0.15 Å, using 13.65 GeV LCLS design energy.

DOI: 10.1103/PhysRevSTAB.13.070702 PACS numbers: 41.60.Cr, 41.20.Gz, 41.50.+h

## I. INTRODUCTION

The x-ray free electron laser based on self-amplified spontaneous emission (SASE FEL [1]) is a state-of-the-art instrument for scientific research with enormous potential and an equally impressive footprint, both in physical scale and cost. However, the cost and complexity of such extensive scientific infrastructure limits the diffusion of this revolutionary 4th generation light source, which promises to allow fundamental investigations of matter at the length and time scale of Angstroms and femtoseconds. The lengths of the LCLS and X-FEL undulators are well over 100 meters [2,3]; the multi-GeV electron injectors are measured in km. The beam energy and thus the accelerator size needed is a function of the desired short FEL wavelength, $\lambda_r \simeq \frac{\lambda_u}{2\gamma^2}[1 + K^2/2]$, where $\gamma$, $\lambda_u$, and $K$ are Lorentz factor, undulator period, and undulator strength parameter, respectively. On the other hand, the overall undulator length is a function of the large gain lengths $L_g$, required to reach saturation. The gain length in the one-dimensional approximation—appropriate to x-ray operation—is given by [4]

$$L_{g,1D} = \frac{\lambda_u}{4\pi\sqrt{3}\rho_{1D}} \tag{1}$$

with the one-dimensional dimensionless gain parameter defined as

$$\rho_{1D} = \frac{1}{\gamma}\left[\frac{I_e}{16I_A}\frac{K^2[JJ]^2}{\sigma_x^2 k_u^2}\right]^{1/3}. \tag{2}$$

One can appreciate the scaling of the gain length with relevant physical parameters from Eqs. (1) and (2), where $\sigma_x$ and $I_e$ are the horizontal beam size and beam current, $I_A$ is the Alfven current ( $\sim 17$ kA for electrons), and $[JJ]$ is short-hand for $[J_0(\xi)\text{-}J_1(\xi)]$ with $\xi = K^2/(4 + 2K^2)$ for the planar undulators used in this paper [5]. Before discussing the beam parameters and their effect on FEL performance *per se*, we note that a shorter period undulator permits a lower cost accelerator to be used, as one mitigates the demanded value of the electron energy $\gamma m_e c^2$. For a given $\lambda_r$, this implies that $\gamma \propto \sqrt{(1 + K^2/2)\lambda_u}$.

Recently, it has been appreciated that one may dramatically increase the beam brightness $B_e = (2I_e)/\epsilon_n^2$, where $\epsilon_n$ is the normalized beam emittance, by using lower charge in the electron injector [6], thus allowing higher quality, denser beams in the undulator. This density increase is accomplished not through higher current—which can be nearly preserved in low-charge operation—but by lower beam sizes, $\sigma_x^2 = \epsilon_n\bar{\beta}/\gamma$, where $\bar{\beta}$ is the Twiss beta function. The higher brightness delivered to the undulator is enabled by the inherent scaling of $\epsilon_n$ and the current at the photocathode source, and also because emittance degrading collective effects are mitigated during emittance compensation [7] and compression [8]. Thus, one may preserve the low emittance obtained at the injector while

*foshea@physics.ucla.edu
†rosen@physics.ucla.edu

 

enhancing the current, yielding unprecedented high brightness.

Enhanced beam brightness has several important implications, arising from growth of the gain parameter $\rho_{1D}$. The first, emphasized in Eq. (1), is that the length of the undulator will be shorter in this case. In this regard, we note that a much more compact FEL undulator is obtained by employing higher beam brightness, thus enhancing $\rho_{1D}$, while one simultaneously lowers $\lambda_u$. According to Eq. (2), this implies not diminishing the value of $K$ too dramatically as $\lambda_u$ is lowered, providing explicit motivation for high field, short period undulators. Further, a compact SASE x-ray FEL based on higher brightness beams is inherently more efficient, as the energy extracted from a beam of total energy $U_b = N_b \gamma m_e c^2$ is approximately $\rho_{1D} U_b$. Thus, one may partially counteract the loss of FEL output energy at lower bunch charge $eN_b$ by more efficiently driving the lasing process. For many FEL applications this is a critical point to consider.

In this paper, therefore, we consider the use of a short period length, $\lambda_u = 9$ mm, cryogenic high field undulator, in tandem with low-charge, high brightness beams, which have been studied both theoretically [6] and experimentally [9] previously. We discuss detailed design simulations of the undulator performance, as well as practical implications surrounding undulator construction. We illustrate by start-to-end simulations of the proposed SPARX FEL at Frascati, the advantages in compactness, lowered beam energy, ultrashort pulse operation and efficiency offered by this combination of novel undulator design and extremely high brightness electron beams. It is shown that the FEL radiation brightness in this case is 2 orders of magnitude higher than that of the LCLS.

The key component of enhanced beam brightness in low-charge operation is, as noted above, the decrease in the emittance. For improved FEL gain the generalized Pellegrini criterion should be followed, which states that $\epsilon_n < \frac{\lambda_r \gamma}{4\pi} \frac{\bar{\beta}}{L_{g,1D}}$, where $\bar{\beta}$ is the average beta function during the lasing process. As $\lambda_r \sim \lambda_u/\gamma^2$, this relation becomes difficult for conventional photoinjector beams to obey at short FEL wavelength, $\lambda_r$. If one can lower the emittance dramatically, unprecedented short wavelengths may be achieved. With a short wavelength undulator, operation at extremely short wavelengths can be accomplished using existing accelerators which produce extremely energetic electron beams. In one example presented in this paper, we show promising operation of a SASE FEL using the LCLS injector in low-charge mode that yields lasing at 0.15 Å. This represents a leap of 1 order of magnitude in photon energy to 83 keV, a coherent x-ray source of unparalleled capabilities in probing dense, high-$Z$ materials.

Small emittance beams can potentially lengthen the lasing gain length by not efficiently replenishing the laser energy that diffracts away from axis. Therefore, the beam emittance should be carefully chosen to balance decreasing the gain length through emittance reduction and laser energy loss through diffraction. The opposing emittance conditions can be summarized with the following three-part inequality [5]:

$$\frac{2L_{g,1D}}{\bar{\beta}} \leq \frac{4\pi\epsilon_n}{\lambda_r \gamma} < \frac{\bar{\beta}}{L_{g,1D}}. \tag{3}$$

When the left inequality in Eq. (3) is strongly satisfied, the electron beam can efficiently feed lasing modes and the result is a potentially transversely incoherent beam in the far field, as undesired higher order transverse modes may be amplified. Barely satisfying this condition means that only the mode with the strongest gain will exist in the far field, presumably the $TEM_{00}$ mode, and transverse coherence is obtained. Strongly violating the left inequality means that diffraction plays a large role in the FEL gain, diminishing it by providing a non-negligible mechanism for the near-axis field to weaken. When the right side of the inequality is violated the electron beam rms divergence is sufficient to introduce significant red shifting of the near-axis emitted photons, thus introducing longitudinal incoherence and damping the gain process, as we shall see. Equation (3) may be used to guide the selection of the undulator and external focusing parameters given an input beam, or vice versa. In this paper we will encounter a variety of design scenarios that illustrate a range of cases in the triple inequality.

As an aside, we note that the combination of the small physical aperture of the undulator and the very short electron beam presents a novel problem in wakefield calculation. Not only does the anomalous skin effect become important [10], but the frequency composition of the charge distribution, and thus the fields, enters the infrared and optical frequencies nearing the transmission window of metals. In addition, the length of the beam and the natural spread of the velocity fields at the metal walls of the undulator become comparable for multi-GeV, fs long beams. An estimate of when the fields become ''velocity field dominated'' can be found by comparing the width of the velocity fields at the wall versus the length of the beam, $S = a/(\gamma\sigma_z)$. The beams we present here all have $S \sim 1$ with the tabletop FEL dominated by the bunch length. The wakefields created under the conditions presented here are currently under investigation.

We begin our discussion in the following section with a description of the undulator design. It should be noted that this design was stimulated first by application to a laser wakefield accelerator (LWFA)-driven FEL at MPQ-Garching [11]. This initiative, in which one is aggressively applying the principle of making the injector compact ($\sim$ cm), one is presently limited in beam energy to $\sim$1 GeV [12]. Thus, in order to produce lasing at short wavelength, a high field, short period undulator is needed.

## II. UNDULATOR DESIGN

All magnets are limited in the strength of the on-axis field they can produce by their magnetic properties. Modern undulators are limited in parameter space ($\lambda_u$, K) by available materials. To decrease the period while maintaining large undulator parameter, the remanence of the available magnetic materials must be increased. A somewhat recent approach adopted to solve this problem is to cool the magnets. Both neodymium-iron-boron (NdFeB) and samarium-cobalt (SmCo) magnets make gains in energy product as they are cooled as cooling limits the size of the domains with undesired magnetization directions. While SmCo's gains are relatively small, continuing to 4.2 K, NdFeB sees large increases in energy product as the material is cooled down to 135 K. At this point the material undergoes a spin-axis reorientation due to competition between anisotropy and exchange forces, the latter being dominant at room temperature, and the useful field created by the magnet begins to drop with continued cooling [13]. Cryogenic undulators using NdFeB have been built, cooling to above the spin-axis reorientation onset [14–16].

The remnant field is not the principal consideration; in order for an in-vacuum undulator to withstand the radiation environment within the vacuum chamber, the coercivity of the material must be sufficiently high. This is a well-known facet of undulator design, with magnet suppliers offering a variety of grades of NdFeB, differing principally in the dysprosium content [17,18]. Because dysprosium increases coercivity at the cost of remanence at room temperature, typically coercivity and remanence are roughly inversely proportional [19]. While permanent magnets show negative temperature gradients of both the remanence and coercivity [18,20], the temperature coefficient of coercivity is much larger than that of remanence. As such, if the magnets are going to be cooled the trade of higher remanence for lower coercivity at room temperature is usually sound as cooling will cause larger gains in coercivity as opposed to remanence.

A recent collaboration has produced a praseodymium (Pr) based permanent magnet that can be cooled to 30 K without the spin-axis reorientation of neodymium magnets [20]. As presented above, the increase in remnant field is accompanied by an even larger increase in coercivity which has been linked to higher radiation resistance [21]. Because of the ability to cool praseodymium magnets to well below the temperatures of NdFeB, these magnets have much higher radiation resistance and, therefore, offer the best performance in in-vacuum insertion devices. Use of these magnets in extremely high brightness electron beam free electron lasers can significantly decrease the length of the undulators required to reach saturation, the magnets are also extremely useful, because of their increased durability, for insertion devices used in high average current synchrotron light sources.

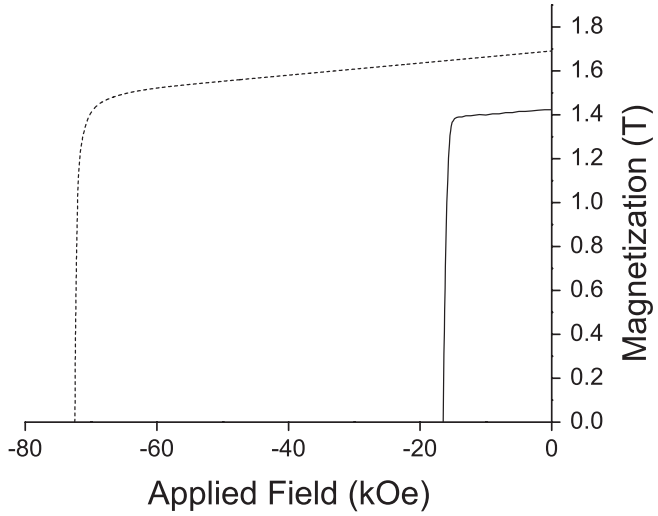


FIG. 1. Magnetization curves for the $(Nd_{0.2}, Pr_{0.8})_2Fe_{14}B$ magnets at 30 K (dashed line) and 300 K (solid line). The large increase in coercivity and energy product when the magnet is cooled can be seen.

The undulator magnets are a rare-earth mix of 80% praseodymium and 20% neodymium added to iron and boron, $(Nd_{0.2}, Pr_{0.8})_2Fe_{14}B$, which are sintered. This is in contrast to the previous praseodymium material used to produce prototype undulators which simply substituted praseodymium in place of neodymium [22–24]. The material has shown modest gains in remnant field and large gains in both coercivity and energy product when cooled to 30 K (see Fig. 1) [20,25]. The undulator poles will be made from vanadium permendur, an alloy with equal parts of Co and Fe and a few percent vanadium, with a saturation induction of 2.34 T.

The undulator is a hybrid design in-vacuum device to allow a very small undulator gap. The hybrid design was chosen because it shows modest gains over a pure permanent magnet device at small gap-to-period ratios [26]. To model the undulator, two 3D codes have been used: RADIA and MAXWELL 3D [27,28]. The result of many simulation and parameter permutations is that the unique combination of small gap, high permeability steel and strong magnets poses a particularly difficult problem for modern magnetostatic solution methods, see Fig. 2. The material magnetization curves are defined identically in MAXWELL 3D and RADIA, with the iron pole magnetization curves taken from RADIA and the magnet magnetization curves coming from fits to measurement [25], indicating that the effects are indeed solution dependent and not the result of differences in material properties. One source of difference between the two packages is the length of the simulated undulator. Because MAXWELL 3D accepts boundary conditions, the model simulated is infinitely long while the RADIA model can only be 4–5 periods long because the segmentation required to accurately model the field in a ~2 mm gap undulator is very large and one quickly runs into onerous

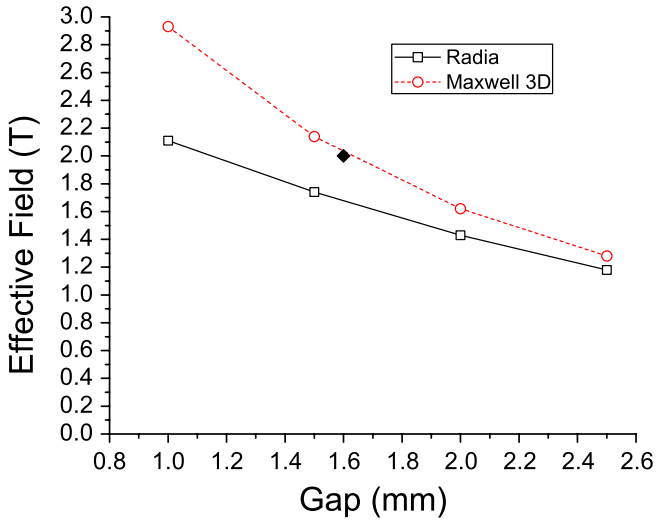


FIG. 2. (Color) Simulation results for the 9 mm period undulator when cooled to 30 K, showing the effective magnetic field, given by $B_{\text{eff}} = \sqrt{\sum(B_n^2/n^2)}$. The difference between the two curves at large gap can be nearly entirely accounted for by the difference in simulated undulator length while segmentation limits in RADIA prevent more accurate comparison at the small gap ($< 2$ mm). The black diamond shows the assumed working point. $K_{\text{eff}} = 0.84 B_{\text{eff}}$.

memory limits. Previous simulations with larger segmentation and larger gaps indicate that the cross talk between magnets diminishes to below simulation precision at about five periods. Therefore, in order to account for all the effects of magnet and pole coupling the simulation region should be at least ten periods long. After the undulator length is taken into account there is still a sizable difference between the simulation results at the smallest gaps which is also likely due to segmentation limits. Because of these factors we have decided to use the Maxwell simulations as the basis for the following FEL simulations.

For the calculations below, the undulator parameter is assumed to be $K = 1.7$, with a 1.6 mm gap, which is indicated in Fig. 2 by the black diamond. A prototype undulator is currently being constructed to measure the effective field. Should the Maxwell results be overly optimistic there are a few techniques for increasing on-axis field, such as side magnets, yet to be employed in the design.

The principal obstacles in undulator construction are the material's coercive weakness at room temperature (see Fig. 1) and the large forces between poles when the undulator gap is small. Two methods have been developed to cope with the coercive delicacy of the magnets during room temperature assembly. The first, more technically challenging, method is to surround the magnets in a SmCo sheath. The second method is to first fill the magnet lattice with dummy magnets which will be replaced one by one with the praseodymium magnets.

### A. Samarium-cobalt sheaths

It is well known that the edges and corners of high permeability materials will act as high flux points when the material is not saturated [29,30]. Because of this, bringing strongly magnetized materials with relatively weak coercivity in contact with iron pieces with sharp edges can result in demagnetized regions. Further, these regions can grow during many heating and cooling cycles as long as the domain walls do not encounter blocking sites whose potential energy prohibits further movement. This can be prevented by properly pre-aging the material, a very common procedure, through higher temperature baking or exposure to external field. In a 9 mm period hybrid undulator the weak coercivity is compounded by the thin magnets: strong, thin magnets act like two narrowly separated plates of charge with fields that attempt to short the potential difference.

The most obvious solution to the so-called corner problem is first to soften the corners and edges with chamfers and then to move the edges of the iron away from the magnets by enlarging the poles. Efficient undulator design, however, requires that the iron poles be smaller than the magnets along any given dimension away from the undulator axis to prevent the iron poles from directing flux away from the beam. The response to this is to replace the

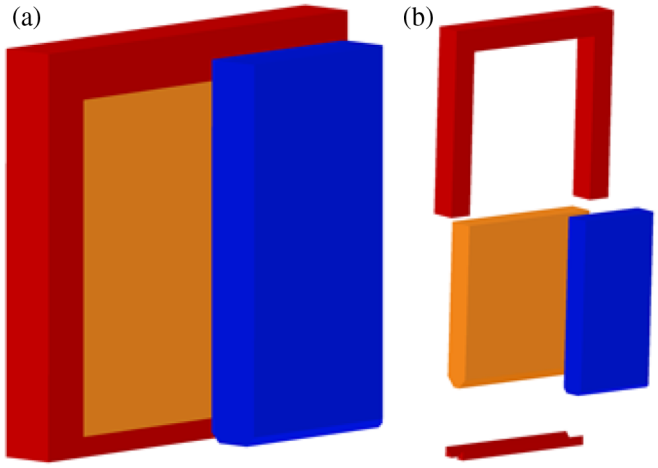


FIG. 3. (Color) Praseodymium magnet design with samarium-cobalt sheath. Part (a) shows one quarter of an undulator period. The red samarium-cobalt sheath surrounds the more easily demagnetized, at room temperature, orange praseodymium magnet. Half of the blue steel pole has been cut away to reveal the structure of the assembly. Part (b) is an exploded view of (a) which shows that the bottom pieces of samarium-cobalt are used to fill in the chamfers of the praseodymium magnet. This is useful because having more strong magnet material near the beam axis promotes field quality. Although the chamfer samarium-cobalt fill-ins are naturally attracted to the praseodymium magnets, some form of adhesive or mechanical restraint will be required. From an engineering standpoint it is easier to replace the fill-ins with a full strip of samarium-cobalt and make the praseodymium magnet a simple block.

magnets near the high flux regions with more resilient magnets (cf. Fig. 3). In this case samarium-cobalt is used because it does not have a spin-axis reorientation down to 4.2 K [20], and it has the highest coercivity of commonly used magnetic materials.

The drawback to this design is finding a reliable way to sheath the magnet using either vacuum, cold safe glue, or mechanically. This problem has yet to be solved. The benefit, however, is a dependable magnet lattice which need not be handled any differently than any other in-vacuum undulator.

### B. Magnetic material replacement

Because of the large forces on the iron poles, when the undulator gap is small, they must be firmly secured to the undulator mounting beam. This means that when this hybrid undulator is assembled the poles are first fixed and then the magnets are inserted. Simulation has shown that this method also results in smaller reverse fields in the inserted magnets. Further, simulation has shown that the insertion of the magnets into a partially empty lattice leads to unacceptably large reverse fields. These increased reverse fields are caused when inserting the $i$th magnet, while the previous slot $(i-1)$ has been filled and the next slot $(i+1)$ remains empty. To correct for this imbalance, all the slots will first be filled with neodymium magnets of comparable strength at room temperature which will then be replaced by the praseodymium magnets. While the neodymium magnets are replaced by the praseodymium magnets, shield plates will be used to further reduce the reverse fields in the praseodymium magnets.

The drawbacks to this design are the construction of throwaway neodymium magnets and the proximity of the edges of the iron poles to the delicate praseodymium magnets. During uncooled periods, the undulator's temperature should be controlled to ensure that the magnets do not get warm enough to demagnetize small regions near the high flux points of the steel poles. Room temperature is acceptable but the quickly diminishing coercivity of the material demands that the temperature not become very much higher.

### C. Field errors and correction

The interference effects of incoherent undulator x-ray sources and the relative phase slip of the microbunching electrons in a free election laser are very sensitive to phase errors caused by errors in the path of the electrons as they pass through the undulator. The relative phase of the far field radiation incident on a detector located on the axis of the undulator is

$$\phi[z] = \omega(t' - z/c) = \frac{2\pi}{\lambda_r}\left(\frac{z}{2\gamma^2} + \frac{1}{2}\int_0^z \beta_x^2(z')dz'\right), \quad (4)$$

where the angle of the particles emitting the radiation is $\beta_x$ with $\beta_x \ll 1$ and $z$ is the distance along the undulator. The phase is a linearly increasing function of distance with a small oscillatory term overlaid. Neglecting the first and second integrals of the particle motion which result in angle and path offset errors, respectively, and can be corrected by appropriate undulator entrance and exit design, we focus here on localized, random path errors which lead to errors in the integral term of Eq. (4) which can be much more pernicious and are more difficult to correct. Following Halbach [31], we fit the MAXWELL 3D curve in Fig. 2, and estimate that a gap error of 13 $\mu$m results in an absolute 0.5% field error between for all sub-$\lambda_u$ gap settings. Because the phase error is cumulative, all random distributions of field error do not equally effect the intensity of the output radiation and the figure of merit that should be used is adequate radiation properties.

To obtain such small gap error there are several approaches that should be used in concert: precision machining of the individual parts, sufficient sorting of pole pieces and pole clamps, and careful undulator support design to ameliorate or even take advantage of thermal effects. The first two methods for coping with gap errors go hand in hand as the small differences in even precision machined parts can be used to compensate for errors in gap that are additive, for instance a depression in the in-vacuum beam can be matched with a taller pole piece. At the same time a special set of pole clamps can be created, either intentionally or otherwise, with an assortment of differing heights to hold the poles in place at the desired height as the poles are naturally pulled out by the forces between the undulator halves. To compensate for the materials shrinking during cooling, it may be necessary to employ mechanical distorting techniques to the undulator such as that used in the SPring-8 design [32].

We note that traditional shimming of the undulator is very difficult as this would require $\mu$m thick foils of magnetically conductive material to be placed with high precision.

Lest the tolerances required to build this undulator seem overwhelming, we note that when compared to the other high field option available at this period length the total tolerances are quite similar while the hybrid device under consideration here has a higher peak field ($B_{\mathrm{peak}} = 0.6$ T) given the same 4.4 mm gap [33]. Although the superconducting design benefits from fewer pieces, high radiation environments will require a great deal of cooling power at the very low superconducting temperatures while a hybrid device cooled to 30–80 K is much easier to keep cool.

## III. EXAMPLES OF FEL PERFORMANCE WITH CRYOGENIC PR-BASED UNDULATOR

As discussed above, there are a wide variety of FEL scenarios that benefit from use of the short period, high field undulator. Further, these FELs have in common the use of very high brightness electron beams. In this section, we illustrate such application in five distinct cases: (1) the

SPARX FEL, in which a ~2 GeV, 1 pC beam is used to create an extremely compact hard x-ray FEL, with harmonics reaching to the current LCLS wavelength; (2) the LCLS beam run at 0.25 pC charge and 4.5 GeV energy, in which one obtains saturation at the current LCLS wavelength in a fraction of the undulator length; (3) the same beam run at 13.65 GeV energy, which enables a >80 keV x-ray FEL; (4) the experimentally studied moderate charge (20 pC) beam case at LCLS, which is compressed to 2 fs, in which the emittance effects are notable, and (5) the original LWFA case, in which one may have a compact "tabletop terawatt" FEL.

### A. SPARX

We discuss here a first example of the exploitation of the 9 mm period, high field undulator introduced above, that of its utilization in the SPARX FEL, currently under design in Frascati. For the beam simulations, we follow the acceleration, compression, and lattice program used in the SPARX technical design report [34]. We concentrate on the case of 1 pC operation, in which sub-fs pulse, single-spike operation at 2 nm fundamental wavelength has been predicted in previous analysis with the standard $\lambda_u = 2.8$ cm undulator [6]. The electron beam is first compressed to $\sigma_z = 4.7$ $\mu$m using velocity bunching, and then chicane compressed to an rms bunch length of $\sigma_z = 0.21$ $\mu$m (0.7 fs) at 1.2 GeV, on the way to acceleration up to a final energy of 2.1 GeV. The beam in this case has extremely low emittances, $\epsilon_{n,x(y)} = 7.5(3.3) \times 10^{-8}$ mrad, and over 700 A peak current after final compression. The larger horizontal emittance is due to coherent synchrotron radiation effects in the chicane. With this limit, the electron beam brightness at the undulator is $B_e = 2 \times 10^{20}$ A-m$^{-2}$ rad$^{-2}$, which should be compared with the nominal high charge ($Q = 1$ nC) baseline design value of $B_e = 2.8 \times 10^{15}$ A-m$^{-2}$ rad$^{-2}$. This dramatic difference in brightness produces quantitatively different behavior in the FEL gain process.

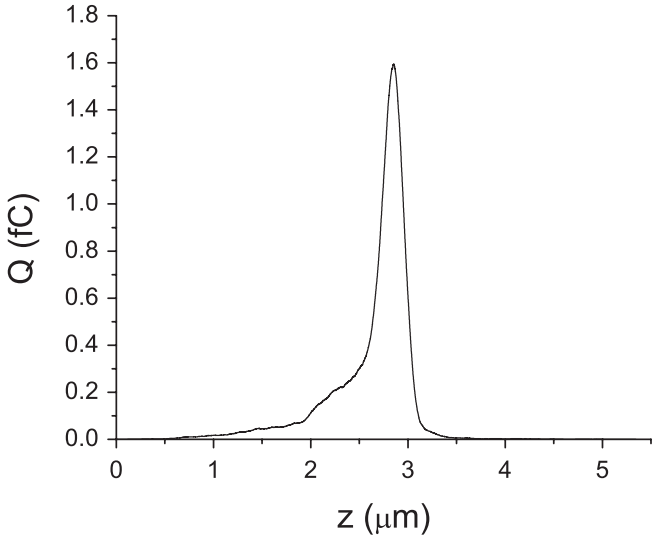


FIG. 4. Beam profile of the SPARX ultrashort beam as generated with start-to-end simulations.

The beam's longitudinal phase space displays multi-fs tails outside of the lasing core, and thus the rms length of the radiation pulse is yet smaller than that of the electron beam, see Fig. 4. In the reference design case discussed in Ref. [6], where an undulator with $\lambda_u = 2.8$ cm and $K = 1.67$, the 2 nm FEL pulse given in GENESIS simula-

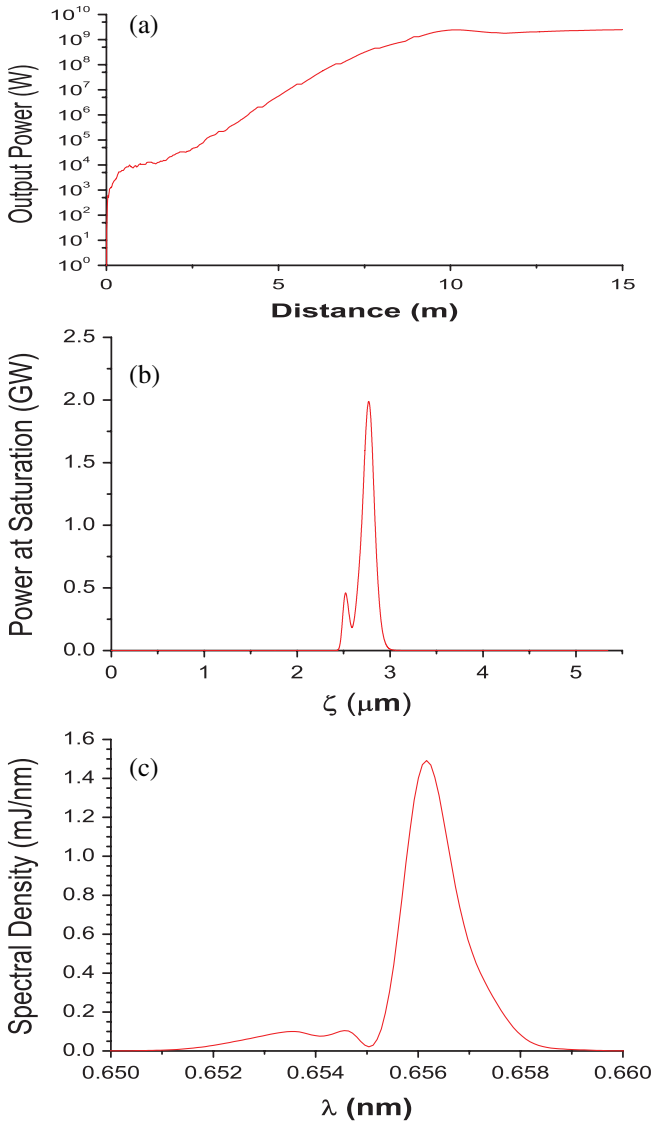


FIG. 5. (Color) GENESIS simulation results for the SPARX ultrashort low-charge case. Part (a) shows the exponential high gain regime saturating at 10 m of undulator, the regions of zero gain are due to the significant gaps between undulators reserved for the strong focusing quadrupoles and diagnostics. Part (b) shows the gain as a function of distance along the beam, the knee in the charge profile (Fig. 4) creates a similar knee in the radiation longitudinal profile. Part (c) shows the spectrum of the output radiation. The radiation has extremely narrow bandwidth.

tions has an rms length of $\sigma_t = 0.48$ fs. This pulse displays only a single spike at saturation, which is achieved in simulation after 30 m. As the beam is significantly higher brightness than that of the high charge baseline design, the saturation length is indeed shorter, decreasing from 50 m in the baseline design case, despite running at higher energy and shorter wavelength, which is 3 nm in the standard case.

With our high field cryoundulator, we employ the same simulation beam particles as utilized in Ref. [6] to evaluate the SASE FEL performance. In comparison to the baseline design, we have decreased the average beta function in the undulator, from 5.5 to 2 m. The tighter focus implied is encouraged by the use of lower emittance beams, as one does not encounter gain degradation from excessive transverse angular motion. The fundamental wavelength is, in this case, 6.56 Å, or a factor of nearly 5 shorter than obtained with the standard undulator. The spectrum at saturation, given by GENESIS simulation, is shown in Fig. 5(c). The evolution of the power along the undulator is illustrated in Fig. 5(a), showing a gain length of 43 cm, and saturation of the fundamental at 10 m. Indeed, with such a short gain length, one may in principle decrease the average beta function in the undulator further. In practice, the lower limit on the beta function is given by the practical consideration of our choice of 1 m undulator sections. Quadratic pole faces will allow for strong focusing and a further decrease in the beta function [35,36]. Nonetheless, the presented scenario is a strikingly compact, high gain system. Despite such a short cooperation length, with a well sub-fs electron beam, quasi-single-spike operation [cf. Fig. 5(b)] is obtained, with an rms x-ray pulse length of 0.35 fs. The peak power is over 2 GW, giving $6 \times 10^9$ photons at 1.8 keV, a photon beam peak brightness of $3 \times 10^{35}$ photons/(s mm$^2$ mrad$^2$ 0.1% BW).

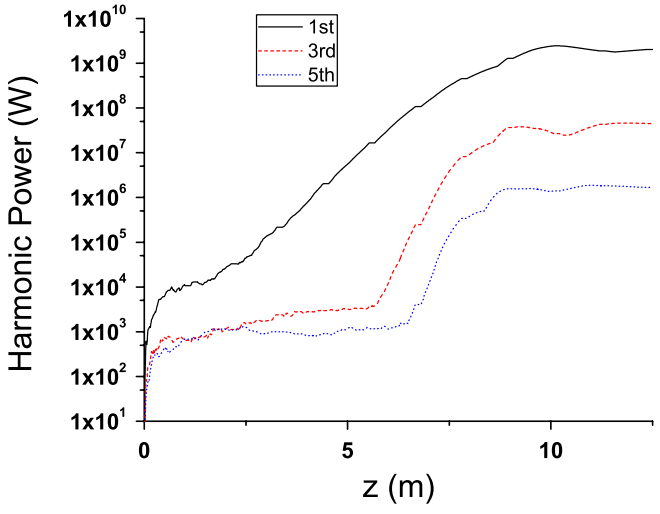


FIG. 6. (Color) Harmonic gain of the SPARX ultrashort low-charge beam lasing in the cryogenic hybrid praseodymium undulator.

Because of the strong gain on the fundamental interaction, the beam is microbunched ever more strongly in the undulator, and the possibility of observing gain on the odd harmonics presents itself [37]. We have studied this phenomenon with GENESIS as well, with the results summarized in Fig. 6. Note that in this case the 5th harmonic has a wavelength of only 1.3 Å; we may create a SASE FEL with wavelength below that of the LCLS using only 2.1 GeV electrons in this short period, high field, high brightness electron beam scenario. This 10-m undulator system produces over $10^6$ coherent hard x-ray photons.

This compact SASE FEL system illustrates well the marriage of our novel cryoundulator design with ultrahigh brightness electron beams produced at low charge. In the following example, we emphasize the possibilities opened not just by the beam brightness, but by the achievement of lower emittance *per se*. We will, from this viewpoint, examine opportunities for pushing the frontier in coherent x-ray production to ever shorter wavelengths.

### B. LCLS ultralow charge, high brightness beam scenario

In order to study possible single-spike behavior in the LCLS, we have examined scenarios based on use of 0.25 pC beams, in which case yet shorter pulses can be achieved. This shortening, in comparison with the SPARX case discussed above, is demanded for single-spike performance at shorter wavelength because the cooperation length is much reduced at the LCLS wavelength of 1.5 Å. In the context of the LCLS injector and linac, we have performed start-to-end simulations in which the beam is compressed to $\sigma_t \simeq 0.2$ fs with a peak current of ~350 A. With such small charge, the beam longitudinal phase space is quite compact, and no significant tails arising from coherent synchrotron radiation during compression are observed in the ELEGANT simulations. The transverse phase space is also more well behaved in the compressor, with all significant emittance growth occurring during velocity bunching; no focusing solenoids are available in the post-gun section of the injector, and the final emittance in both transverse planes is in this case $\epsilon_n = 3.3 \times 10^{-8}$ mrad. Thus the beam is slightly brighter than in the 1 pC case discussed above, while the four-dimensional transverse phase space area is diminished by over half. This will prove to be a key advantage in pushing the FEL to lase at unprecedented short wavelengths, well sub-Angstrom.

To illustrate first the effect of beam brightness and a short period undulator, we study the use of the cryogenic undulator in the same configuration as in the previous section to investigate SASE FEL performance near the nominal LCLS wavelength, but obtained at a lower energy of 4.5 GeV. The results of the GENESIS simulation of this scenario are shown in Figs. 7(a)–7(c). Figure 7(a) shows the evolution of the SASE power along the undulator, in which case we note saturation achieved within 15 m, with a

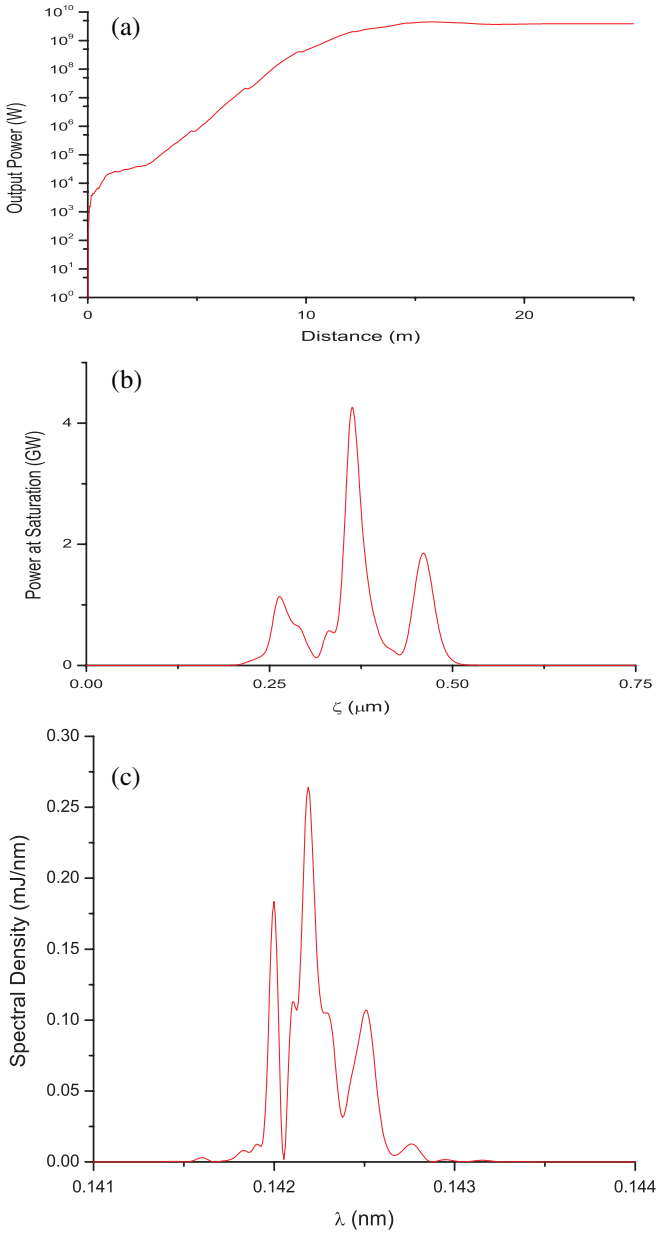


FIG. 7. (Color) (a) GENESIS simulation results for the 4.5 GeV LCLS beam. The saturation length of the fundamental mode is 15 m with a gain length of 70 cm. (b) At saturation the beam shows three spikes in the longitudinal profile, consistent with a 11 nm cooperation length [45]. (c) The fundamental interaction wavelength is just over 1.42 Å.

gain length $L_g = 70$ cm. These parameters are a factor of 6–7 shorter than achieved in the LCLS standard undulator, high charge case. Despite use of charge 3 orders of magnitude smaller than in the LCLS nominal operating regime, a peak power of 5 GW is achieved in this simulation, corresponding to $2 \times 10^9$ 1.42 Å photons in less than 0.5 fs FWHM.

With such high gain, and thus shortened cooperation length, the beam does not lase in single-spike mode in this case, as seen in Fig. 7(b), but rather has roughly three spikes. These spikes are also displayed, as expected, in the wavelength spectrum shown in Fig. 7(c). One may recover single-spike performance by running at higher charge, with (perhaps purposefully enlarged) higher emittance.

We note that in this case the electron beam emittance remains a factor of ~25 below the generalized Pellegrini criterion. Thus, one may envision use of higher energy beams with shorter wavelength operation than that expected of the LCLS. In fact, what is particularly striking about the LCLS-derived examples is perhaps not the possibility of dramatic shortening of the undulator and use of lower energy beams, but extending the wavelength reach of the FEL. As an aside we see that, given the scaling of Eq. (3) with energy, the middle term is the fastest growing term and that means that increasing the energy of the beam cannot decrease the transverse coherence of the output radiation, if all the other factors are held constant. As such, we have studied use of a nearly full energy, 13.65 GeV, electron beam at the LCLS in tandem with the cryogenic undulator. In this case we expect lasing at a fundamental wavelength of 0.15 Å, or exactly 1 order of magnitude shorter than the LCLS design. At this energy and wavelength, the beam used is much closer to the Pellegrini emittance limit, about a factor of 4. The photons at this wavelength have an energy of 83 keV, and lie in a spectral region of high interest for studies of dense, high-$Z$ materials, and may form the basis of large future FEL initiatives [38]. Such incredible x-ray energy can only be achieved by an electron beam with a very small emittance, such as the beams we present here, in order to prevent energy spread caused by quantum fluctuations in the emitted synchrotron radiation to quench the lasing process [39,40].

To simulate this ultrashort wavelength system, we introduce 2.27 m long undulator sections, with quadrupole focusing to give an average focusing $\bar{\beta} = 4.8$ m. The performance of this FEL is a prime example of the new possibilities afforded by use of high brightness beam, short period undulator system: the gain length at 0.15 Å is only 2.46 m [Fig. 8(a)], and yielding saturation in 40 m. The saturated power in this case is over 2 GW, with about $10^8$ photons per pulse. The spectral coherence of this source is as expected for SASE, with the temporal [Fig. 8(b)] and wavelength power distributions both showing approximately eight spikes, reflecting the number of cooperation lengths (4 nm, or 14 attoseconds) inside of the lasing pulse.

Lasing at such short wavelengths is indeed predicated on the emittance being as small as predicted from the start-to-end simulations. To illustrate this, we utilize the beam parameters achieved at SLAC in the first attempt to examine low-charge, high brightness beam performance [41]. In this case, while the peak current is increased to an estimated 8 kA, the geometric mean of the transverse emittances is also over an order of magnitude higher, as noted

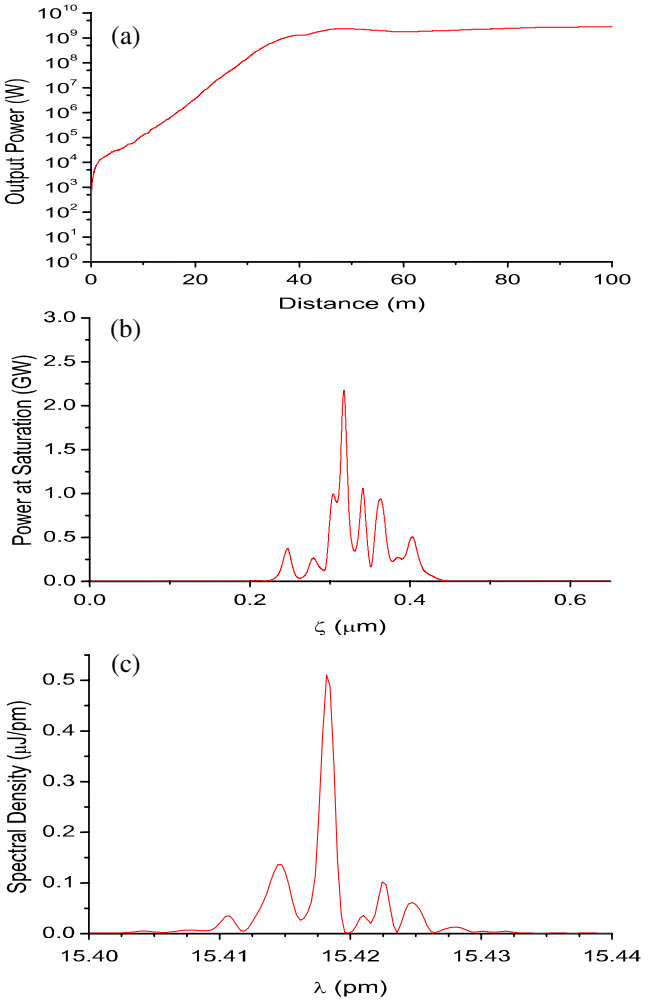


FIG. 8. (Color) (a) GENESIS simulation of a 13.65 GeV LCLS beam traveling through the cryogenic high field undulator. Saturation occurs in 40 m. The incredibly short fundamental wavelength, 0.15 Å (c), does not allow single-spike operation (b).

above. Thus the beam brightness is degraded, and more importantly, the Pellegrini criterion is quite strongly violated. As such the SASE FEL gain simulated in GENESIS using our cryoundulator design is also degraded, with the results shown in Fig. 9. Here one would need a 150 m undulator to approach saturation, which is a much less desirable scenario than given by use of the higher brightness beam. Thus it is advisable to push towards lower charges and therefore emittances, as studied in Ref. [6].

Alternatively, one can regain compliance with the generalized Pellegrini criterion by lowering, as studied in the extreme low-charge case above, the beam energy. With the electron energy set to 4.5 GeV and the same emittance and peak current, one lases at the nominal LCLS wavelength (1.5 Å), as before, and saturates the FEL at approximately 15 GW peak power in 20 m of undulator. The evolution of the SASE FEL power in GENESIS simulation of this case is shown in Fig. 10. A similar exercise in examining the

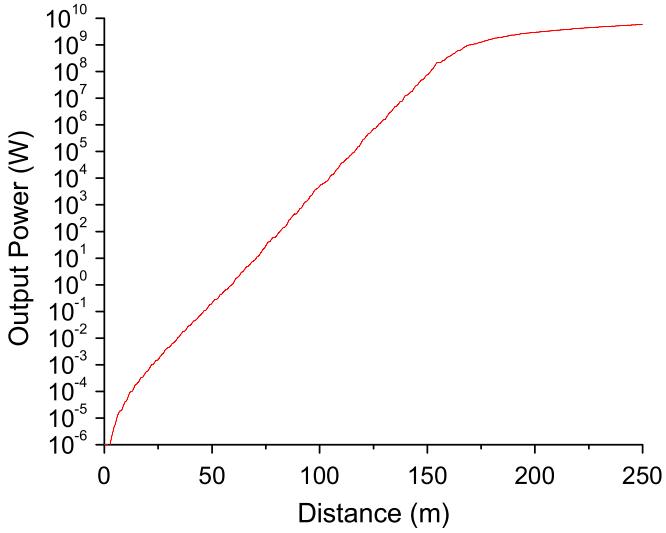


FIG. 9. (Color) GENESIS simulation of the 20 pC, 2 fs rms pulse length beam at LCLS, full LCLS energy (14.3 GeV). Violation of the Pellegrini criterion causes dramatic growth in the gain length.

performance of the 20 pC beam was reported in Ref. [41] using the existing LCLS undulator. In this case, the 4.3 GeV beam produces a saturating FEL within 25 meters, at a wavelength of 1.5 nm. This comparison nicely demonstrates the advantage of using the short wavelength cryogenic undulator.

### C. Tabletop FEL based on laser wakefield accelerator

The original motivation of the undulator design work discussed in Sec. II was the desire to build an x-ray SASE FEL with a very compact footprint by utilizing a laser

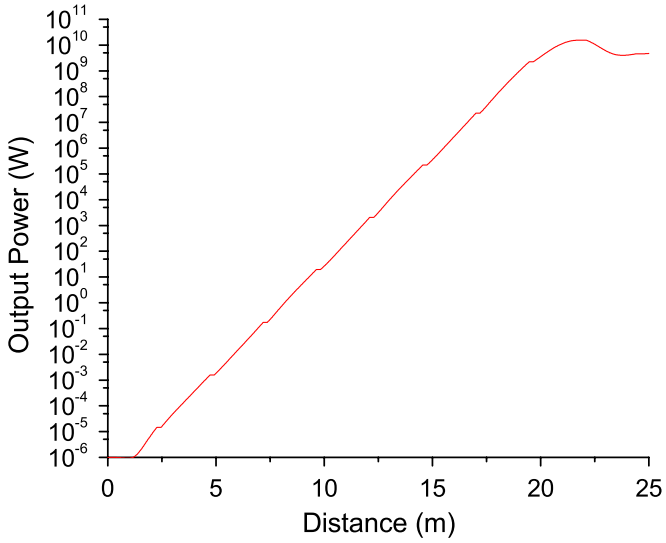


FIG. 10. (Color) GENESIS simulation of the LCLS 20 pC beam at derated energy of 4.5 GeV, compliance with Pellegrini criterion reestablished.

wakefield accelerator (LWFA) as the injector. This injector is currently being used in a soft x-ray undulator light source [42]. In such a scheme, one with $>10$ GV/m field driven by an ultrashort (10's of fs) laser pulse, may create $>$ GeV electron beams in a dense plasma a few cm in length. This approach is discussed in depth in Refs. [11,43]. To explore the performance of the current undulator design as applied to this scheme, we use the beam parameters given in [11] for the beam expected from the LWFA driven by a 1 PW laser pulse: 160 kA peak current contained in a 4 fs rms pulse, $\epsilon_n = 1 \times 10^{-6}$ mrad, energy of 1.74 GeV, with rms energy spread of 0.1%. The beam here is quite bright, competitive with the 0.25 pC LCLS case given above, due to the extremely high predicted current. This is an important distinction. The previous examples show the importance of meeting the Pellegrini criterion by controlling the electron beam emittance and thus settling for lower total bunch charge. The result of using only these electrons best tuned to the exponential gain process is a quickly saturating free electron laser. In the current tabletop case, however, the opposite approach of brute force has been taken. This free electron laser saturates in a short distance because an enormous number of electrons have been crowded into a rather typical emittance. Therefore, the electrons can constructively add energy to the fundamental mode much faster than diffraction effects can take energy away. This further means that there will be many transverse radiation modes in the far field.

The GENESIS simulation results for this case are given in Figs. 11(a)–11(c). They display extremely high gain at a wavelength near 0.95 nm, with a peak saturation power of over 1 TW, well in excess of the 58 GW predicted for the design discussed in Ref. [11]. The total saturated pulse energy is impressive, reaching 6.5 mJ, or $3 \times 10^{13}$ soft x-ray (1.3 keV) photons. This highly energetic saturation state, further, occurs within 3 m of the undulator. Because of the enormous current in this example and the small undulator gap assumed (1.6 mm), the wakefields produced by the front of the beam will disrupt the lasing process. To avoid this problem the undulator will need to be tapered. This presents the opportunity to use the natural dependence of the remnant field on the temperature of the magnets to adjust the field in sections of the undulator, temperature tapering. Care must be taken to account for the expansion of the materials as a function of temperature [32].

This example serves well in illustrating a vision of an ultracompact FEL design, one in which the injector is a compact LWFA section, and an undulator that is over an order of magnitude shorter than those in use today. This compelling scenario, should it be realized, will produce the first ever terawatt FEL, and it will fit in a university-scale lab. One might term it, in the tradition of today's ultrafast laser systems and the LWFA initiative described in Ref. [11], a *tabletop terawatt* ($T^3$) SASE FEL.

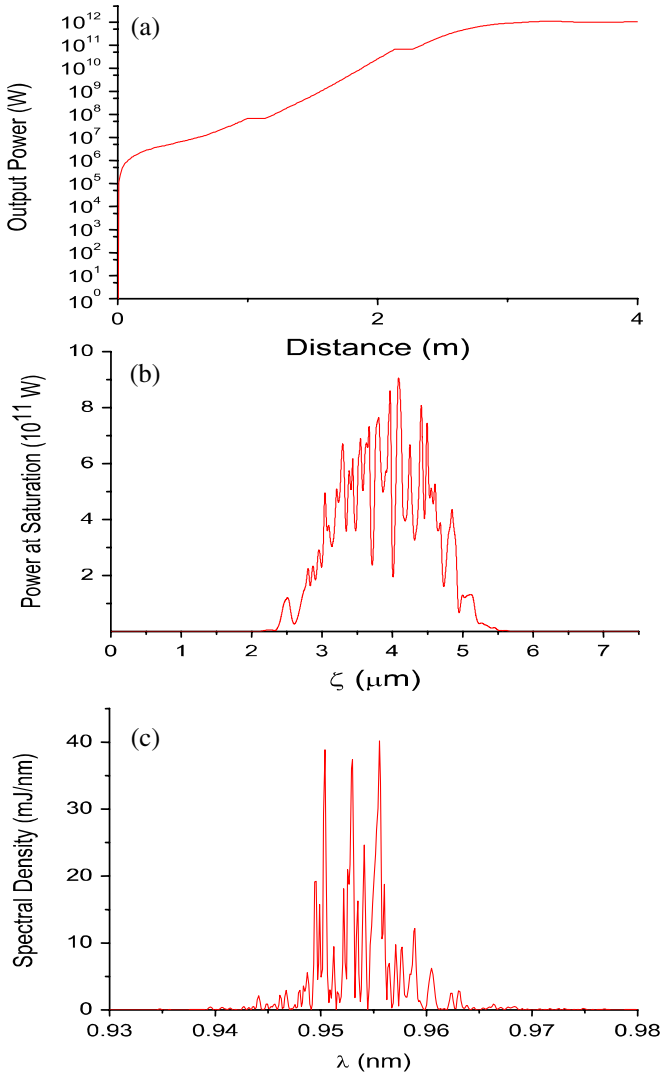


FIG. 11. (Color) GENESIS results for the ($T^3$) SASE FEL. (a) Saturation occurs in 3 m. (b) The soft x-ray energy is distributed fairly uniformly over the entire length of the pulse. (c) The spectral makeup if the beam is noisy, expected from such a large emittance beam.

## IV. CONCLUSIONS

The cryogenic undulator under development for use as a tabletop free electron laser has some challenging technical difficulties but shows enormous promise to make the current frontier of x-ray free electron laser brightness available to more users. Through careful electron beam brightness control at the photocathode gun we have shown a marked decrease in the saturation length of proposed free electron lasers (Table I). Simulation shows a great deal of flexibility of the undulator with operation modes that include harmonic generation (SPARX), few spike operation (SPARX and LCLS operating at 4.5 GeV), ultrahard x-ray operation (LCLS at 13.65 GeV), and terawatt soft x-ray laser production (tabletop FEL).

TABLE I. Summary of the results of the GENESIS free electron laser simulations.

| | | SPARX | | LCLS | | $(T)^3$ FEL |
|---|---|---|---|---|---|---|
| $E$ | GeV | 2.1 | 4.5 | 13.65 | 13.65 | 1.74 |
| $I$ | kA | 0.7 | 0.35 | 0.35 | 8.0 | 160 |
| $Q$ | pC | 1.0 | 0.25 | 0.25 | 20 | 1600 |
| $\epsilon_{n,x(y)}$ | $10^{-8}$ mrad | 7.5(3.3) | 3.3(3.3) | 3.3(3.3) | 40(14) | 100(100) |
| $\lambda_r$ | Å | 6.5 | 1.4 | 0.15 | 0.15 | 9.5 |
| $\bar{\beta}$ | m | 2.0 | 4.8 | 4.8 | 4.8 | 4.3 |
| $\rho$ | $10^{-3}$ | 1.8 | 0.75 | 0.36 | 0.51 | 3.6 |
| $L_{\mathrm{sat}}$ | m | 10 | 15 | 40 | 170 | 3 |
| Output power | GW | 2.4 | 4.5 | 2.4 | 1.0 | 1090 |

Recently, emittance exchange between a short longitudinal slice and the horizontal has been proposed using a $\mathrm{TEM}_{10}$ laser mode in an undulator [44]. We note that the fundamental difference between this technique and the one presented here is that emittance exchange uses a standard photocathode beam and an extra element in the beam line while we use high brightness electron beams produced at the cathode. The principle result remains that higher brightness beams allow higher brightness free electron lasers produced in shorter undulators.

## ACKNOWLEDGMENTS

The authors wish to thank Sven Reiche for his many helpful observations, and Claudio Pellegrini for useful discussions. This work supported by the U.S. Department of Energy under Contracts No. DE-FG02-07ER46272 and No. DE-FG03-92ER40693, the Office of Naval Research under Contract No. ONR N00014-06-1-0925, the DFG Cluster of Excellence "Munich-Centre for Advanced Photonics" (MAP), and Transregio TR 18.

[1] R. Bonifacio, C. Pellegrini, and L. M. Narducci, Opt. Commun. **50**, 373 (1984).
[2] J. Arthur *et al.* (Linac Coherent Light Source), Stanford Linear Accelerator Center Report No. SLAC-R-593, 2002.
[3] M. Altarelli *et al.* (European XFEL), DESY Report No. DESY 2006-097, 2006.
[4] R. Bonifacio, C. Pellegrini, and L. M. Narducci, Opt. Commun. **50**, 373 (1984).
[5] Z. Huang and K. J. Kim, Phys. Rev. ST Accel. Beams **10**, 034801 (2007).
[6] J. B. Rosenzweig *et al.*, Nucl. Instrum. Methods Phys. Res., Sect. A **593**, 39 (2008).
[7] L. Serafini and J. B. Rosenzweig, Phys. Rev. E **55**, 7565 (1997).
[8] Y. S. Derbenev, J. Rossbach, E. L. Saldin, and V. D. Shiltsev, DESY Report No. TESLA-FEL 95-05, 1995.
[9] S. Reiche, P. Musumeci, C. Pellegrini, and J. B Rosenzweig, Nucl. Instrum. Methods Phys. Res., Sect. A **593**, 45 (2008).
[10] G. Reuter and E. Sondheimer, Proc. R. Soc. A **195**, 336 (1948).
[11] F. Grüner *et al.*, Appl. Phys. B **86**, 431 (2007).
[12] W. P. Leemans *et al.*, Nature Phys. **2**, 696 (2006).
[13] D. Givord, H. S. Li, and R. Perrier de la Bâthie, Solid State Commun. **51**, 857 (1984).
[14] J. Chavanne *et al.*, Synchrotron Radiat. News **22**, 34 (2009).
[15] J Chavanne *et al.*, in Proceedings of the Synchrotron Radiation Instrumentation Conference, Melbourne, Australia, 2009 (to be published).
[16] T. Tanaka *et al.*, Phys. Rev. ST Accel. Beams **12**, 120702 (2009).
[17] M. Hasegawa *et al.*, J. Magn. Magn. Mater. **124**, 325 (1993).
[18] T. Hara *et al.*, Phys. Rev. ST Accel. Beams **7**, 050702 (2004).
[19] R. D. Brown and J. R. Cost, Trans. Magn. Soc. Jpn. **25**, 3117 (1989).
[20] K. Uestuener *et al.*, in Proceedings of the 20th Workshop on Rare Earth Permanent Magnets and Applications, Knossos, Greece, 2008.
[21] O. P. Kähkönen, S. Mäkinen, M. Talvitie, H. Rajainmäki, and M. Manninen, Europhys. Lett. **12**, 413 (1990).
[22] T. Tanaka *et al.*, J. Synchrotron Radiat. **14**, 416 (2007).
[23] T. Tanabe *et al.*, in *Proceedings of the 11th European Particle Accelerator Conference, Genoa, 2008*, edited by I. Andrian (EPS-AG, Genoa, Italy, 2008).
[24] T. Tanabe *et al.*, in Proceedings of the Synchrotron Radiation Instrumentation Conference, Melbourne, Australia, 2009 (to be published).
[25] J. Bahrdt *et al.*, in Proceedings of the Synchrotron Radiation Instrumentation Conference, Melbourne, Australia, 2009 (to be published).
[26] J. Chavanne and P. Elleaume, in *Undulator, Wigglers and Their Applications*, edited by H. Onuki and P. Elleaume (Taylor & Francis, London, 2003).
[27] P. Elleaume, O. Chubar, and J. Chavanne, in *Proceedings of the Particle Accelerator Conference, Vancouver, BC, Canada, 1997*, edited by J. Thomson (IEEE, New York, 1997).
[28] www.ansoft.com.
[29] J. D. Jackson, *Classical Electrodynamics* (John Wiley & Sons, New York, 1999).

[30] F. O'Shea *et al.*, in *Proceedings of the 23rd Particle Accelerator Conference, Vancouver, Canada, 2009*, edited by M. Comyn (IEEE, Piscataway, NJ, 2009).
[31] K. Halbach, J. Phys. (Paris) **44**, C1-211 (1983).
[32] T. Tanaka *et al.*, Phys. Rev. ST Accel. Beams **12**, 120702 (2009).
[33] I. Ben-Zvi *et al.*, Nucl. Instrum. Methods Phys. Res., Sect. A **318**, 781 (1992).
[34] L. Palumbo *et al.* (SPARX FEL), SPARX-FEL Technical Design Report, 2009.
[35] E. T. Scharlemann, J. Appl. Phys. **58**, 2154 (1985).
[36] G. Travish and J. Rosenzweig, Nucl. Instrum. Methods Phys. Res., Sect. A **345**, 585 (1994).
[37] A. Tremaine *et al.*, Phys. Rev. Lett. **88**, 204801 (2002).
[38] B. Carlsten (private communication).
[39] J. Rossbach, E. L. Saldin, E. A. Schneidmiller, and M. V. Yurkov, Nucl. Instrum. Methods Phys. Res., Sect. A **374**, 401 (1996).
[40] S. Reiche, E. L. Saldin, E. A. Schneidmiller, and M. V. Yurkov, in *Proceedings of the Workshop on Single Pass, High Gain, FELs Starting from Noise, Aiming at Coherent X-rays, Garda Lake, Italy, 1997*, edited by R. Bonifacio and W. A. Barletta (American Institute of Physics, New York, 1997), p. 29.
[41] Y. Ding *et al.*, Phys. Rev. Lett. **102**, 254801 (2009).
[42] M. Fuchs *et al.*, Nature Phys. **5**, 826 (2009).
[43] F. Grüner *et al.*, Phys. Rev. ST Accel. Beams **12**, 020701 (2009).
[44] D. Xiang, Phys. Rev. ST Accel. Beams **13**, 010701 (2010).
[45] R. Bonifacio, L. De Salvo, P. Pierini, N. Piovella, and C. Pellegrini, Phys. Rev. Lett. **73**, 70 (1994).